

An Acid Response IR780-Based Targeted Nanoparticle for Intraoperative Near-Infrared Fluorescence Imaging of Ovarian Cancer

Jiao Song ^{*}, Huixia Ye^{*}, Senwei Jiang, Yuebo Yang, Xiaomao Li

Gynaecology Department, The Third Affiliated Hospital of Sun Yat-sen University, Guangzhou, 510630, People's Republic of China

^{*}These authors contributed equally to this work

Correspondence: Yuebo Yang; Xiaomao Li, Gynaecology Department, The Third Affiliated Hospital of Sun Yat-sen University, Guangzhou, 510630, People's Republic of China, Tel/Fax +86 20-85252259; +86 20-85253289, Email yangyueb@mail.sysu.edu.cn; Lixmao@mail.sysu.edu.cn

Introduction: Complete resection of all visible disease (R0 resection) is critical for the treatment of ovarian cancer patients, and accurate real-time guidance provided by intraoperative near-infrared (NIR) fluorescence images is beneficial for achieving complete resection of all visible disease.

Methods: Based on the optical properties of IR780 and the characteristics of the acidic tumor microenvironment, we develop a new smart nanoparticle (eg, FA-IR780&PFOB-SNPs) by using the pH response nano framework (FA-PEG-PLGA-PEOz) and adjusting the amount of IR780. The FA-IR780&PFOB-SNPs was characterized for morphology, microstructure, particle size, pH-response, drug-loading efficiency and biological safety. The ultraclear fluorescence Navigation Endoscopy System was applied to evaluate the tumor recognition of FA-IR780&PFOB-SNPs in vivo.

Results: The structure of FA-IR780&PFOB-SNPs was stable in a neutral environment, and the near-infrared (NIR) fluorescence was turned off, while the structure of FA-IR780&PFOB-SNPs was degraded in the acidic tumour microenvironment, and the NIR fluorescence was turned on. Through the ovarian subcutaneous xenograft tumour and ovarian intraperitoneal xenograft tumour models, it was confirmed that FA-IR780&PFOB-SNPs could clearly display the boundaries of abdominal micron-sized tumours through near-infrared fluorescence imaging, with a TBR greater than 5.

Conclusion: The FA-IR780&PFOB-SNPs have the potential to provide to ovarian cancer intraoperative near infrared fluorescence navigation during precision tumour resection to achieve R0 and improve the prognosis of ovarian cancer patients.

Keywords: near-infrared fluorescence imaging, IR780 iodide, epithelial ovarian cancer, tumour-activatable nanoparticles

Introduction

Epithelial ovarian cancer is the leading cause of cancer-related death in gynaecology patients.¹ Due to a lack of effective screening options and specific warning signs, over 75% of patients are diagnosed with stage III/IV disease. Surgery is the cornerstone in the initial treatment of ovarian cancer.² It was reported that the median survival time of patients who undergo complete resection of all visible disease (R0) is 99.1 months, and the corresponding durations for patients with residuals of 0.1–1 cm or >1 cm are 36.2 or 29.6 months, respectively.³ Additionally, the lower residual tumour load that is obtained by using optimal cytoreductive surgery can improve subsequent systemic treatments, including chemotherapy and molecular targeted therapy (poly(ADP-ribose) polymerase (PARP) inhibitors).⁴ However, it has been difficult to achieve R0 by relying solely on palpation and visual inspection by surgeons. Moreover, surgeons always underestimate residual disease; despite complete surgery, early postoperative computerized tomography detects suboptimal (>1 cm) residual tumours in almost half of patients.⁵

In recent years, some preclinical and clinical studies have shown that fluorescent-guided surgery (FGS, use of tumour-targeted fluorescent dyes to illuminate malignant tissue and thereby facilitate its surgical resection) has promise for

decreasing residual tumours and improving patient outcomes.⁶ Indocyanine green (ICG), a near-infrared fluorescent dye already in clinical use, has been shown to successfully detect metastatic sentinel lymph nodes in breast cancer, cervical cancer, and endometrial cancer,^{7,8} but there was a high rate of false-positives when used in patients with ovarian cancer.⁹ In order to show ovarian tumours clearly by NIR fluorescence imaging during operation, some nanoparticle probes have been designed and achieved excellent results in basic experimental stage.^{10–13} A Phase II clinical trial indicated that OTL38, which consists of folate conjugated to an indocyanine green-like (excitation at 776 nm, emission at 796 nm) near-infrared fluorescent dye termed S0456, was more effective in detecting tumours when using NIR fluorescent imaging during surgery. At least one additional lesion was detected in 48.3% of patients (14/29) by using OTL38-mediated near-infrared fluorescence imaging, but the tumour-to-background fluorescence signal ratio (TBR) of OTL38 was 4.4 ± 1.4 .^{14,15} Some researchers have suggested that tumours can be reliably identified when the TBR is greater than 5.¹⁶

In our previous study, we developed a nanoparticle that is loaded with IR780 iodide (IR780, with better fluorescence imaging ability than ICG) on the basis of folate-modified liposomes for NIR fluorescence image-guided surgery and photothermal therapy in ovarian cancer. In ovarian subcutaneous xenograft tumour models, this nanoparticle significantly increased the fluorescence signals from tumours through the enhanced penetrability and retention effect of nanoparticles and the active targeting effect of folate (studies have confirmed that approximately 76–89% of epithelial ovarian cancers overexpressed the folate receptor).¹⁷ However, due to the optical property of IR780, there was also considerable fluorescence in surrounding normal tissues, and the TBR was only 2.40 ± 0.19 .¹⁸ To decrease the fluorescence signal from the background and improve the TBR, some tumour-activable fluorescence probes (ie, turn-on probes) were designed based on the tumour microenvironment and the optical characteristics of fluorescent molecules, such as SiNc-PNP, which is activated by the acidic microenvironment, and LUM015, which is activated by cysteine cathepsins.^{19,20}

Herein, we developed a tumour-activatable fluorescent smart nanoparticle based on 1) IR780 with excellent fluorescence imaging ability and an aggregate fluorescence self-quenching effect; 2) Poly (lactic-co-glycolic-acid) modified with folate, poly (2-ethyl-2-oxazoline), and poly (ethylene glycol) (FA-PEOz-PEG-PLGA), as a nanocarrier with active tumour-targeting, acid-responsive, biodegradability and histocompatibility properties;^{21,22} 3) perfluorooctyl bromide (PFOB), which is conducive to the formation and stability of nanoparticles ([Figure S1](#)), demonstrated with CT imaging ability in our prior study.²³ The developed smart nanoparticles (FA-IR780&PFOB-SNPs) were engineered to be nonfluorescent in normal tissues due to IR780 self-quenching in nanoparticles, while the IR780 fluorescence recovery in tumours was due to the disassembled nanoparticles ([Figure 1](#)). In this work, we reported that 1) the acid-responsive FA-IR780&PFOB-SNPs, 2) FA-IR780&PFOB-SNPs exhibited better fluorescence imaging abilities than ordinary non-acid responsive IR780-loaded folate-targeted nanoparticles in both subcutaneous and intraperitoneal xenograft human ovarian cancer murine models, especially in intraperitoneal xenograft models, and 3) FA-IR780&PFOB-SNPs recognized submillimetre-scale peritoneal metastases during surgery with higher TBRs.

Materials and Methods

Materials

Poly (lactic-co-glycolic-acid) modified with folate, and poly (ethylene glycol) (FA-PEG4000-PLGA10000) and Poly (lactic-co-glycolic-acid) modified with poly (2-ethyl-2-oxazoline) (PLGA10000-PEOz) were purchased from Xian Rulxi Biological Technology CO., Ltd.(Xian, China). IR780, PFOB and poly (vinyl alcohol) (PVA) were purchased from Sigma-Aldrich (MO, USA). Cell Counting Kit-8 (CCK8) was purchased from Dojindo (Japan). 1,1'-Dioctadecyl-3,3,3',3'-tetramethylindocarbocyanineperchlorate (DiI), Mito-Tracker Green and paraformaldehyde were obtained from Beyotime Technology (Shanghai, China). Deionized water was obtained from a Millipore water purification system. All reagents were used without further purification.

Synthesis of FA-IR780-PFOB-SNPs

FA-IR780&PFOB-SNPs were generated by dissolving FA-PEG4000-PLGA10000, PLGA10000-PEOz, and IR780 at a weight ratio of 12mg:12mg: 2mg in 2 mL of dichloromethane in a tube. Then, 200 μ L of PFOB was added to the mixture and emulsified in an ice-water bath with an ultrasonic probe (Sonics and Materials, Inc., USA) with an amplitude

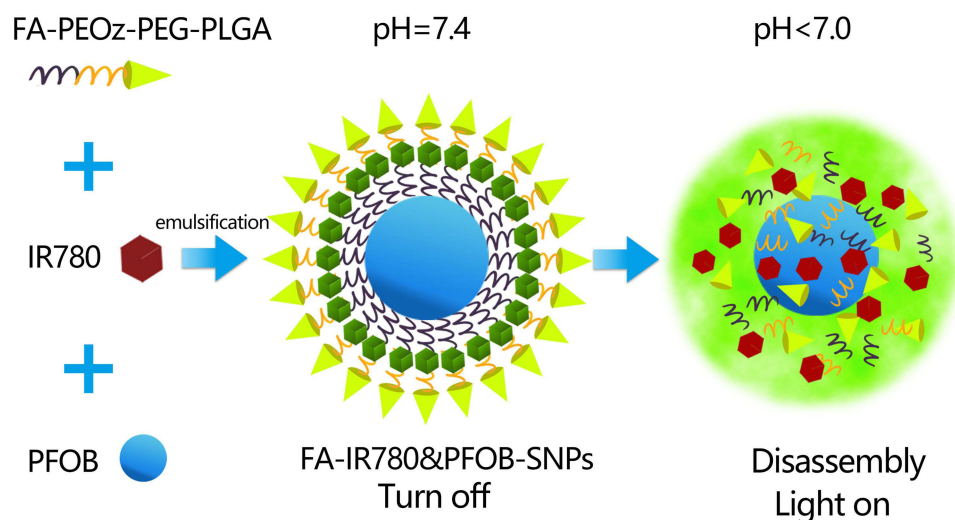


Figure 1 Schematic illustration of the acid-responsive nanoparticles (FA-IR780&PFOB-SNPs).

of 40% for 4 min (5 s on and 5 s off). Next, PVA solution (5 mL, 1% w/v) was added to the emulsion and emulsified in an ice-water bath with an amplitude of 40% for 4 min (5 s on and 5 s off). The final emulsion was stirred for 4 h with a magnetic stirrer (85–2A, Yuexin, Changzhou, China) to extract the dichloromethane. Next, FA-IR780&PFOB-SNPs were isolated from micro-sized NPs by differential centrifugation (Beckman Avanti J-26 XP, Beckman, USA) at 1000 rpm for 5 min and 10,000 rpm for 10 min. Finally, the FA-IR780&PFOB-SNPs were resuspended in PBS at a concentration of 2.5 mg/mL and stored at -20°C . Non-tumour responsive nanoparticles FA-IR780&PFOB-NPs (without PLGA10000-PEOz) and FA-PFOB-SNPs (without IR780) were fabricated by following the same procedure.

Characterization of FA-IR780&PFOB-SNPs

The absorbance of free IR780, FA-PFOB-SNPs and FA-IR780&PFOB-SNPs in dimethylsulfoxide (DMSO) or PBS were recorded on a multifunctional microplate reader (SpectraMax M5, Molecular Devices, San Jose, USA). The standard concentration curve was calculated based on the absorption peak of different concentrations of free IR780 (4, 8, 12, 16, 20, 24 $\mu\text{g}/\text{mL}$) in DMSO.

$$\text{IR780 loading (\%)} = \frac{\text{weight of the IR780}}{\text{weight of the FA - IR780 - PFOB - SNPs}} \times 100\%$$

FA-IR780&PFOB-SNPs were incubated under different conditions for 24 h, which included 4°C PBS at pH 7.4, 37°C PBS at pH 7.4 and 4°C PBS at pH 4.0. Then, the size distributions of the FA-IR780&PFOB-SNPs were measured with a NanoSight NS300 (Malvern Instruments, Malvern, United Kingdom), and the morphology of FA-IR780&PFOB-SNPs was visualized by transmission electron microscopy (TEM, HT-7700, Hitachi, Japan).

NIR Fluorescence FA-IR780&PFOB-SNPs in vitro

The FA-IR780&PFOB-SNPs were directly diluted with foetal bovine serum (FBS) at pH 7.4 or FBS at pH 4.0 (eg, 2.5, 1.25, 0.625, 3.1×10^{-1} , 1.6×10^{-1} , 7.8×10^{-2} , 3.9×10^{-2} , 2.0×10^{-2} , 9.8×10^{-3} , 4.9×10^{-3} , 2.4×10^{-3} , and 1.3×10^{-3} mg/mL). Different concentrations of FA-IR780&PFOB-SNPs were added to black 96-well plates and detected by an in vivo IVIS imaging system (Perkin Elmer, USA) with a 745/840 nm excitation/emission wavelength filter.

Cell Lines and Culture

SKOV3 cells were purchased from ProCell Company (Wuhan China) and cultured in ATCC-recommended media, McCoy's 5A, with 10% FBS (PAN-Biotech, Germany) and 1% penicillin/streptomycin and incubated at 37°C with 5% CO_2 .

In vitro Toxicity

SKOV3 cells were separately cultured in a 96-well plate at a density of 5×10^3 cells/mL in each well. After 24 h of culture, the cells were washed 2 times with PBS, and 100 μ L of medium containing different concentrations of FA-IR780&PFOB-SNPs (eg, 0 μ g/mL, 20 μ g/mL, 40 μ g/mL, 60 μ g/mL, 80 μ g/mL, 100 μ g/mL, and 120 μ g/mL; n = 6 per group) was then added prior to incubating the cells for 24 h. Next, CCK-8 was used to determine cell viability. Briefly, 10 μ L of CCK-8 solution was added to each well and incubated with the cells for 1 h. Then, the absorbances were recorded at 450 nm using a microplate reader (Bio Tek, USA).

Assessment of the in vitro Mitochondria-Targeting Ability

SKOV3 cells were separately cultured in confocal dishes at a density of 5×10^4 cells/mL in each well. After 24 h of culture, the cells were washed 3 times with PBS, and a medium containing 40 μ g/mL DiI-labelled FA-IR780&PFOB-SNPs and DiI-labelled FA-PFOB-SNPs was then added (n= 3 per group). After 2 h of incubation, the cells were washed with PBS and stained with mito-tracker Green for an additional 45 min. After removing the mito-tracker Green, the cell medium was added, and the stained cells were imaged by laser confocal scanning microscopy. The resulting PC coefficients were measured.

Toxicity in vivo and Pharmacokinetic Study

All animal studies were approved and performed in accordance with the animal ethics committee of Sun Yat-Sen University and the national guidelines on the care and use of laboratory animals. Six- to eight-week-old female BALB/c mice were randomly grouped and treated once with different doses of FA-IR780&PFOB-SNPs (eg, 10, 30, and 50 mg/kg) that were administered by intraperitoneal injection (n = 3 per group). The control group received 200 μ L of PBS. The survival rates of the animals were observed 2 weeks after administration. At 14 d, the mice were sacrificed, and the organs (eg, hearts, livers, spleens, lungs and kidneys) were harvested for haematoxylin-eosin (H&E) staining.

For the pharmacokinetic study, blood samples from BALB/c mice were collected at different time points (eg, 0, 0.5, 2, 24, 48 and 72 h; n = 3 per group) after intravenous administration of FA-IR780&PFOB-SNPs (10 mg/kg). The blood IR780 concentrations were measured with a multifunctional microplate reader. The pharmacokinetic statistical parameters were calculated using a noncompartmental model, Drug and Statistics 2.0 (DAS 2.0, Bio. Guider Co., Shanghai, China).

Animal Model

To establish ovarian subcutaneous xenograft tumour models, BALB/c female nude mice were subcutaneously injected with SKOV3 cells (2×10^6 cells in 100 μ L of PBS) on the back. Tumour sizes were assessed every 5 d with a calliper and by using the following formula: $0.5 \times \text{width}^2 \times \text{length}$. When the tumour sizes reached approximately 100 mm³, the mice were used for further experiments.

To establish the ovarian intraperitoneal xenograft tumour model, BALB/c female nude mice were intraperitoneally injected with SKOV3 cells (2×10^6 cells in 100 μ L of PBS) into the abdominal cavity.

NIR Fluorescence and Biodistribution in vivo

The ovarian subcutaneous xenograft tumour mice were randomly divided into two groups: the FA-IR780&PFOB-SNPs group and control group (IR780-loaded folate-targeted ordinary nanoparticles) (n = 3 per group). Compared to the FA-IR780&PFOB-SNPs, the dye loading of IR780 in control group was lower (1.46 \pm 0.01%) and without PLGA-PEOz, the fluorescence always on. After intraperitoneal injection of FA-IR780&PFOB-SNPs (10 mg/kg; the corresponding IR780 dose was 0.35 mg/kg) and FA-IR780 &PFOB-NPs (23.65 mg/kg; the corresponding IR780 dose was 0.35 mg/kg), the mice were imaged with the in vivo IVIS imaging system at the indicated time points (eg, pre-injection and at 1, 3, 24 and 72 h postinjection) after being anaesthetized with pentobarbital sodium salt. The mice were sacrificed at 72 h postinjection, and the major organs, including the intestines, hearts, livers, spleens, lungs, kidneys, and tumours, were dissected for imaging. The corresponding fluorescence intensities were analysed with IVIS software.

Intraoperative Navigation for in vivo Tumours

BALB/c female nude mice harbouring subcutaneous xenografts of SKOV3 tumours were intraperitoneally injected with 10 mg/kg FA-IR780&PFOB-SNPs. The mice were anaesthetized at 72 h ($n = 3$ per group), and the skin overlying the tumours was removed. The surgical areas were imaged in real time by using an ultraclear fluorescence Navigation Endoscopy System (FIONavi4K, Guangdong, China). The tumours and adjacent tissues were removed by navigating with an ultraclear fluorescence Navigation Endoscopy System for pathological examinations. The pathological sections were observed under an inverted fluorescence microscope. The corresponding fluorescence intensities were analysed with ImageJ software.

BALB/c female nude mice harbouring intraperitoneal xenografts of SKOV3 tumours were intraperitoneally injected with 10 mg/kg of FA-IR780&PFOB-SNPs. The mice were anaesthetized at 72 h ($n = 3$ per group), the abdominal skins were incised, and the abdominal areas were opened. The surgical areas were imaged in real time with an ultraclear fluorescence Navigation Endoscopy System. The tumours and adjacent tissues were removed by navigating with an ultraclear fluorescence Navigation Endoscopy System for pathological examinations. The pathological sections were observed under an inverted fluorescence microscope. The corresponding fluorescence intensities were analysed with ImageJ software.

Results

In previous research, we found that IR780 has excellent fluorescence imaging abilities and an aggregate fluorescence self-quenching effect; at higher concentrations, the fluorescence signal decreased with increased concentrations.¹⁸ The principle of the fluorescence self-quenching effect has been reported to be that as the distance between fluorescent molecules decreases, energy transfer among molecules occurs, and the fluorescence is quenched, while when the distance between fluorescent molecules increases, fluorescence recovers.¹⁹ Therefore, we assumed that fluorescence quenched (turned off) nanoparticles could be synthesized by increasing the amount of IR780 in the nanoparticles and decreasing the distance between the IR780 molecules.

After fixing the amount of the nanocarriers FA-PEG-PLGA and PLGA-PEOz, 1 mg, 2 mg, 3 mg, and 4 mg of IR780 were added separately to prepare the nanoparticles. When the initial IR780 doses of 3 mg and 4 mg, the collected nanoparticles showed some precipitation and free IR780. When the IR780 doses were 1 mg and 2 mg, the collected nanoparticles could disperse effectively in PBS. As shown in [Figure 2A](#) and [B](#), there was a significantly stronger fluorescence signal with an initial dosage of 1 mg IR780, while the intensity of the fluorescence signal decreased significantly with an initial IR780 dosage of 2 mg, which suggested that the increased amount of IR780 in the nanoparticles quenched the fluorescence. However, the fluorescence signal of the nanoparticles did not continue to decrease with increased initial IR780 dosages, and there were no significant differences in the intensities of the fluorescence signals between dosages of 2 mg and 3 mg or between dosages of 2 mg and 4 mg. Hence, our study used FA-IR780&PFOB-SNPs with an initial IR780 dosage of 2 mg to perform the subsequent experiments. Free IR780 exhibited an absorbance peak at 795nm ([Figure S2A](#)), and the absorbance peak intensity increased linearly with increased concentrations ([Figure S2B](#)). The absorption spectra were scanned with a multifunctional microplate reader and exhibited an absorption peak at 795 nm ([Figure 2C](#)) which indicated the IR780 was successfully loaded into nanoparticles. According to the calibration curve ($Y=0.0789x+0.0768$) for IR780, the dye loading of IR780 was calculated to be approximately $3.46\pm 0.03\%$ when the initial IR780 dosage was 2 mg ([Figure S1C](#)). At the same time, it was also observed that the drug loading of IR780 was not significantly improved when the initial dosage was increased from 2 mg to 3 mg.

To detect whether FA-IR780&PFOB-SNPs were pH responsive, we dispersed FA-IR780&PFOB-SNPs under different conditions for 24 hours and then determined the particle sizes with a NanoSight NS300 instrument. As shown in [Figure 2D](#), the size was 291.20 ± 82.70 nm when FA-IR780&PFOB-SNPs were dispersed in PBS with pH 7.4 at 4°C; the size was 285.8 ± 76.8 nm when FA-IR780&PFOB-SNPs were dispersed in PBS with pH 7.4 at 37°C; and the size decreased to 115.50 ± 28.00 nm when FA-IR780&PFOB-SNPs were dispersed in PBS with pH 4.0 at 37°C. The results confirmed that the FA-IR780&PFOB-SNPs were pH-responsive, and the increased temperature had a slight effect on the FA-IR780&PFOB-SNPs size. The FA-IR780&PFOB-SNPs exhibited spherical core/shell structures, as observed by TEM. Consistent with the above results, the size of FA-IR780&PFOB-SNPs was significantly reduced in PBS with pH 4.0 at 37°C compared to PBS with pH 7.4 at 4 °C, while the FA-IR780&PFOB-SNPs size did not change significantly in PBS with pH 7.4 at 37°C

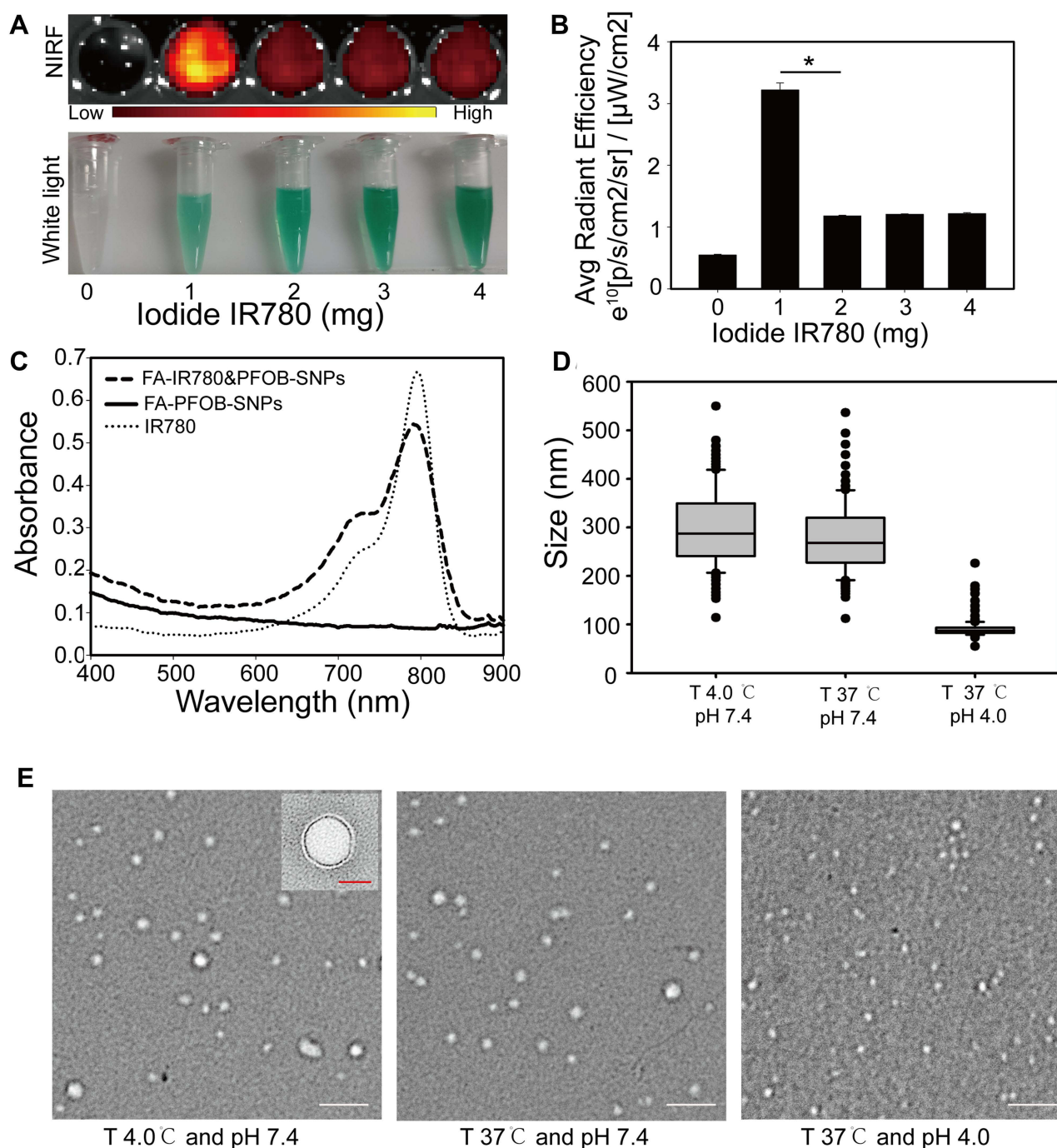


Figure 2 Features of FA-IR780&PFOB-SNPs: **(A)** White light image and near-infrared fluorescence (NIRF) image of FA-IR780&PFOB-SNPs with different dosages of IR780 (eg, 0, 1, 2, 3, and 4 mg); **(B)** corresponding NIRF intensities of FA-IR780&PFOB-SNPs with different IR780 dosages (eg, 0, 1, 2, 3, and 4 mg). Values are expressed as the mean \pm SD, $n = 3$ per group. $*P < 0.05$; **(C)** Absorbance spectra of FA-IR780&PFOB-SNPs, FA-PFOB-SNPs, IR780 in PBS; **(D)** Size distributions of FA-IR780&PFOB-SNPs under differing conditions, including at 4°C PBS with pH 7.4 for 24 h, 37°C PBS with pH 7.4 for 24 h, and 4°C PBS with pH 4.0 for 24 h; **(E)** TEM images of FA-IR780&PFOB-SNPs under differing conditions, including 4°C PBS with pH 7.4 for 24 h, 37°C PBS with pH 7.4 for 24 h, and 4°C PBS with pH 4.0 for 24 h; the white scale bars represent 200 nm, and the red scale bar represents 40 nm.

compared to PBS with pH 7.4 at 4°C (Figure 2E). Notably, the sizes of FA-IR780&PFOB-SNPs that were determined by TME were smaller than those determined by the NanoSight NS300 instrument. This difference between the two methods may be related to the detection principles, and similar results have been reported previously.²⁴

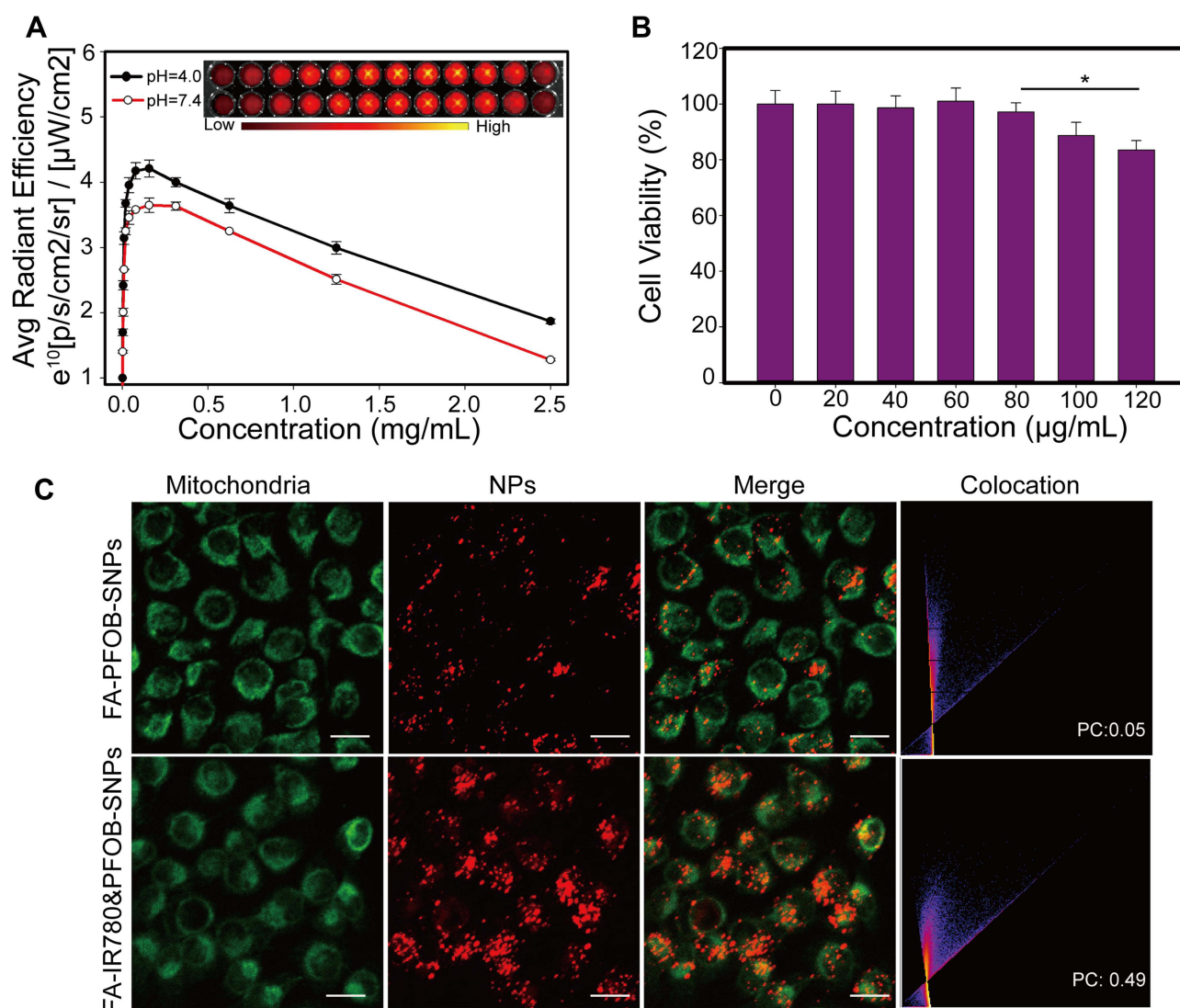


Figure 3 In vitro properties of FA-IR780&PFOB-SNPs: **(A)** Fluorescence imaging and corresponding intensities of FA-IR780&PFOB-SNPs with different concentrations dissolved in FBS at pH 4.0 or at pH 7.4; the values are expressed as the mean \pm SD, $n = 3$ per group; **(B)** SKOV3 cell viabilities after incubation with various concentrations of FA-IR780&PFOB-SNPs for 24 h; the values are expressed as the mean \pm SD, $n = 6$ per group, $*P < 0.05$; **(C)** Mitochondrial location of FA-IR780&PFOB-SNPs and FA-PFOB-SNPs as monitored by MitoTracker; the scale bars represent 50 μm .

In the above experiments, the structure of FA-IR780&PFOB-SNPs with acid responsiveness was confirmed, and the NIR fluorescence imaging abilities were further evaluated. As shown in Figure 3A, the NIR fluorescence signals of FA-IR780&PFOB-SNPs with different concentrations were stronger when dispersed in FBS at pH 4.0 than when dispersed in FBS at pH 7.4. The aggregate fluorescence self-quenching effect of the IR780 is due to the decrease of the distance between the fluorescent molecules, and the change of the concentration in the solution would have the same effect. Hence, a similar trend can be observed for the concentration-dependent fluorescence intensity for nanoparticles dissolved in FBS at pH 4, and 7.4. The fluorescence intensity of FA-IR780&PFOB-SNPs increased rapidly with the concentration at lower concentrations, while the fluorescence intensity decreased slowly with the concentration at higher concentrations, which indicated a concentration-dependent quenching phenomenon.

Next, the tumour cell toxicity of FA-IR780&PFOB-SNPs was investigated using a CCK-8 assay. A 24-h incubation of FA-IR780&PFOB-SNPs (20 $\mu\text{g/mL}$ to 80 $\mu\text{g/mL}$) exhibited negligible toxicity with respect to SKOV3 cell viability, while the cell viability decreased significantly when the incubation dosage of FA-IR780&PFOB-SNPs was 120 $\mu\text{g/mL}$ (Figure 3B). The dose-related tumour toxicity is probably related to the higher dosage of IR780, which has previously

been reported.²⁵ In our previous study, IR780-loaded nanoparticles were demonstrated to have mitochondrial targeting capabilities in mouse breast cancer cells.²⁶ In this study, we examined whether FA-IR780&PFOB-SNPs also have mitochondrial targeting capabilities in ovarian cancer cells. As depicted in Figure 3C, compared with FA-PFOB-SNPs (without IR780), IR780 caused the FA-IR780&PFOB-SNPs to enter cells more rapidly and were more distributed in the mitochondria, which is consistent with the results of a previous study.

Ovarian cancer spreads mainly by intraperitoneal implantation and forms metastases of different sizes in the intra-abdominal cavity (eg, submillimetre to ~10 cm). Intraperitoneal injections of FA-IR780&PFOB-SNPs can passively accumulate in ovarian peritoneal tumours in addition to the active targeting ability that is mediated by folate, especially for submillimetre lesions without tumour angiogenesis.¹⁶ Therefore, intraperitoneal injections were used for the following in vivo experiments. First, we examined the in vivo safety of FA-IR780&PFOB-SNPs. As shown in Figure 4A and B, negligible fluctuations in body weight and H&E staining of the main organs were observed after intraperitoneal administration of different FA-IR780&PFOB-SNPs dosages to healthy female mice, which demonstrated that doses of FA-IR780&PFOB-SNPs below 50 mg/kg caused no significant toxicity in the tested period. Next, the in vivo

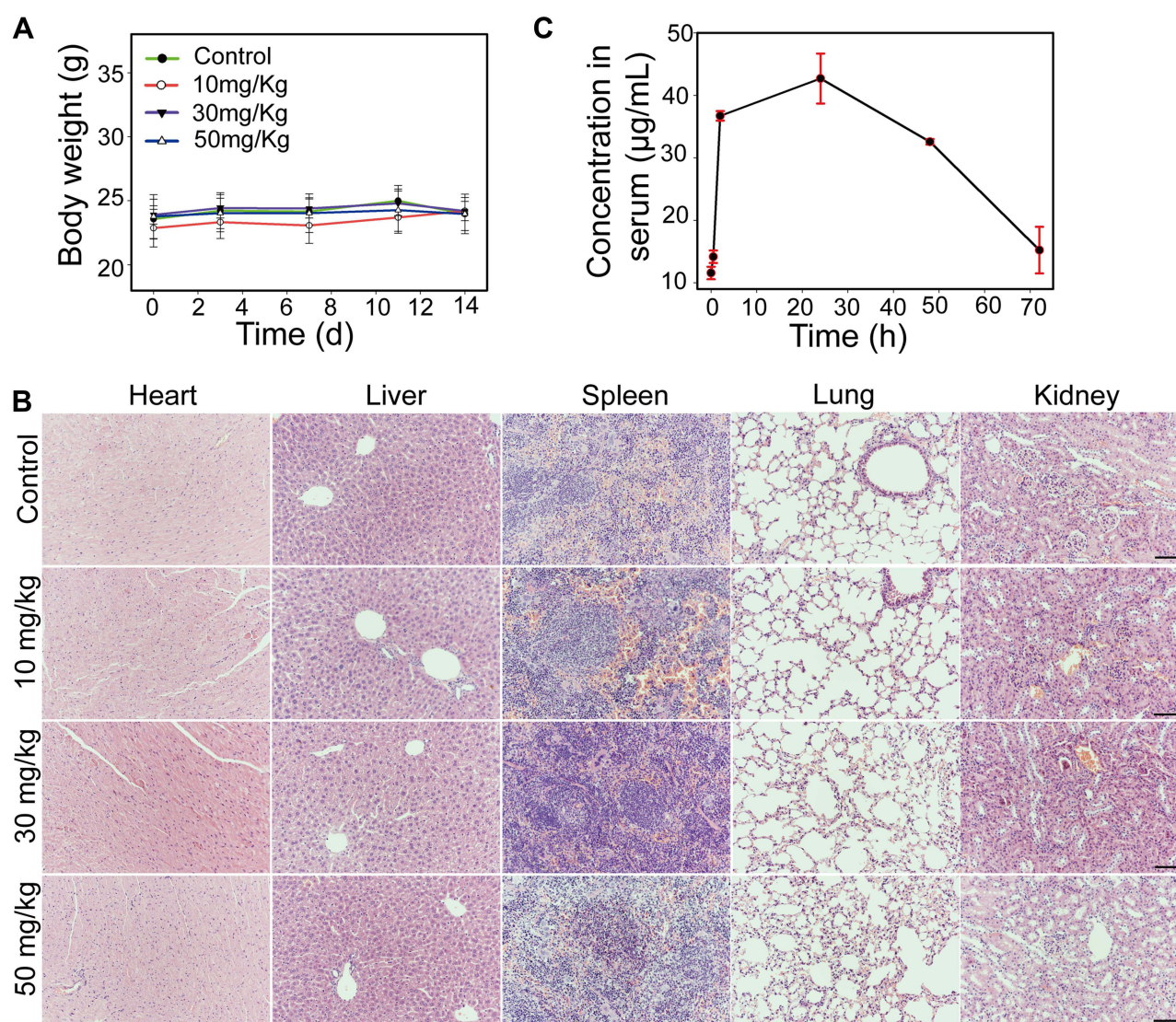


Figure 4 In vivo properties of FA-IR780&PFOB-SNPs: **(A)** Body weight curves of mice after treatment with PBS or 10 mg/kg, 30 mg/kg or 50 mg/kg of FA-IR780&PFOB-SNPs, n = 3 per group. **(B)** Organ tissues of mice were stained with H&E after 14 d of treatment with PBS or 10 mg/kg, 30 mg/kg or 50 mg/kg of FA-IR780&PFOB-SNPs. The scale bars represent 50 µm, n = 3 per group. **(C)** Plasma concentration-time curves after intraperitoneal injection of 10 mg/kg FA-IR780&PFOB-SNPs. Values are the mean \pm SD, n = 3 per group.

pharmacokinetics of FA-IR780&PFOB-SNPs were evaluated. Healthy female BALB/c nude mice were intraperitoneally administered 10 mg/kg of FA-IR780&PFOB-SNPs. As depicted in Figure 4C, the FA-IR780&PFOB-SNPs serum concentration peaked at approximately 24 h, and the half-life of FA-IR780&PFOB-SNPs was 40.16 ± 10.88 h, which indicated that FA-IR780&PFOB-SNPs could be nearly eliminated within 9 days.

To further evaluate FA-IR780&PFOB-SNPs for in vivo NIR fluorescence imaging of ovarian cancer, mice with subcutaneous SKOV3 tumours were first used because subcutaneous tumours are easier to observe and detect. In previous studies, we confirmed that the NIR fluorescence imaging ability of IR780-loaded folate-targeted ordinary nanoparticles (fluorescence always on nanoparticles) was better than that of ICG, free IR780 and IR780-loaded nanoparticles (without folate targeting).^{18,23} Hence, we compared the in vivo NIR fluorescence imaging abilities of FA-IR780&PFOB-SNPs and IR780-loaded folate-targeted ordinary nanoparticles (as control group). Compared to the FA-IR780&PFOB-SNPs, the dye loading of IR780 in control group was lower ($1.46 \pm 0.01\%$) and without PLGA-PEOz, the fluorescence always on. After the mice with subcutaneous SKOV3 tumours were intraperitoneally administered FA-IR780&PFOB-SNPs (10.00 mg/kg, the corresponding IR780 dose was 0.35 mg/kg) and FA-IR780&PFOB-SNPs (23.65 mg/kg, the corresponding IR780 dose was 0.35 mg/kg, as the control group), NIR fluorescence pictures were obtained at different points by the in vivo IVIS imaging system. As depicted in Figure 5A, the background NIR fluorescence signals of the FA-IR780&PFOB-SNPs group were obviously weaker than those of the control group and displayed the tumour earlier. Comparing the mean fluorescence signal intensities in tumours and surrounding normal tissues (TBR), the TBRs of the FA-IR780&PFOB-SNPs group were higher than

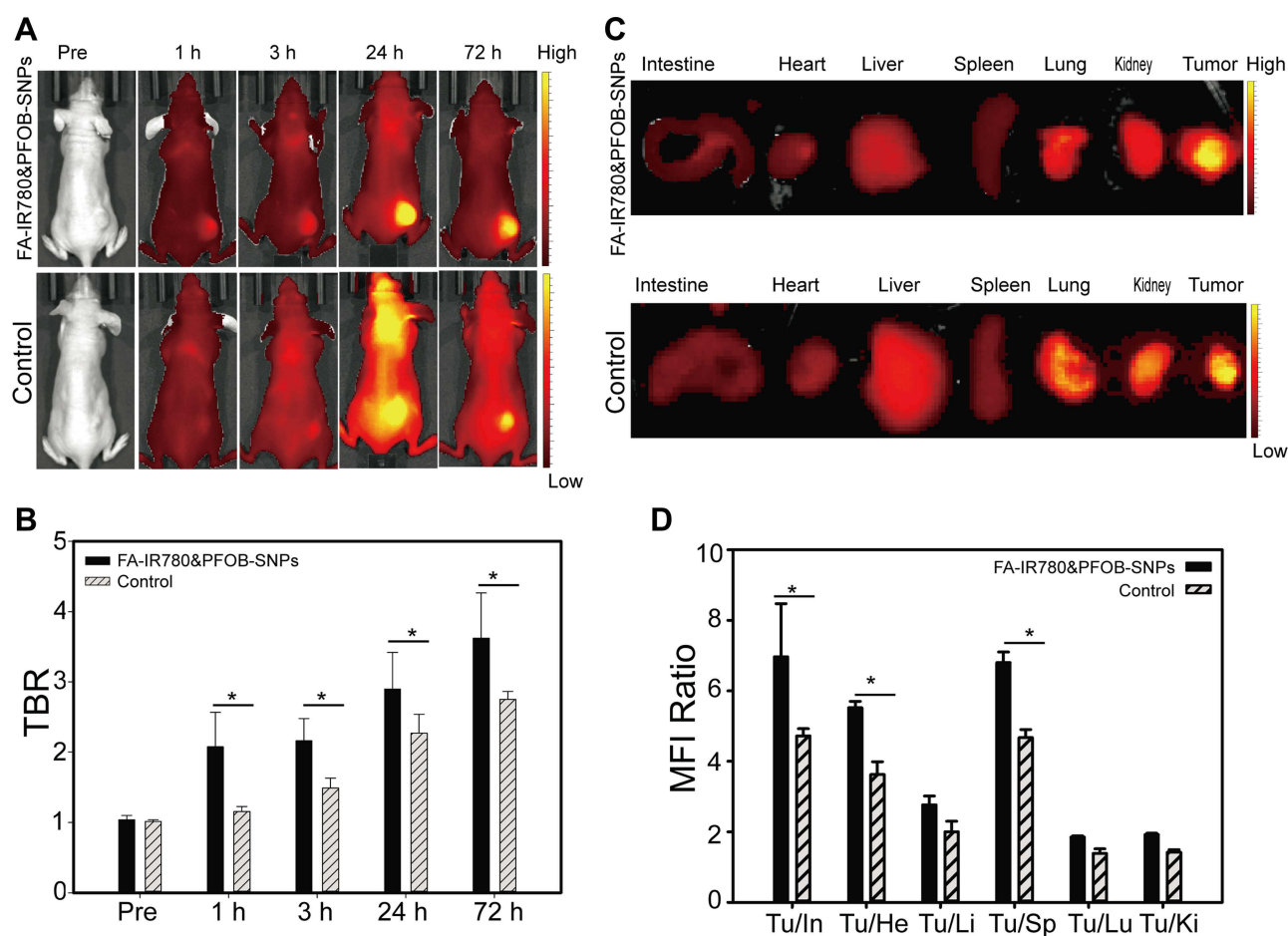


Figure 5 FA-IR780&PFOB-SNPs demonstrated excellent tumour targeting ability in vivo. (A) NIR fluorescence imaging of tumour-bearing mice after intraperitoneal administration of control NPs (eg, FA-IR780&PFOB-SNPs always turned on and without pH response) or FA-IR780&PFOB-SNPs (Smart NPs with pH response) at different time points (eg, pre, 1 h, 3 h, 24 h, and 72 h). (B) TBRs of Control NPs and FA-IR780&PFOB-SNPs at the different time points. (C) Ex vivo fluorescence imaging of mouse major organs and tumour nodes at 72 h; (D) MFI ratios between tumours and organs at 72 h. Values are expressed as the mean \pm SD, n = 3 per group. *P < 0.05.

those of the control group at different points (Figure 5B). To further assess the FA-IR780&PFOB-SNPs distributions, tumours and major organs (eg, intestine, heart, liver, spleen, lung and kidney) were collected and imaged by the in vivo IVIS imaging system at 72 h post-administration. The images obtained both from the FA-IR780&PFOB-SNPs and control groups showed enhanced fluorescence signals in tumours, which indicated effective accumulations of both FA-IR780&PFOB-SNPs and IR780-loaded folate-targeted ordinary nanoparticles in SKOV3 tumours (Figure 5C). Comparing the mean fluorescence signal intensities (MFI) in tumours and normal organ tissues, the MFI ratio of FA-IR780&PFOB-SNPs was higher than that of the control group, especially in terms of the intensity (6.95 ± 1.50), which is always involved in intraperitoneal implantation of ovarian cancer (Figure 5D).

Furthermore, to mimic intraoperative scenarios and evaluate the intraoperative imaging feasibility when using FA-IR780&PFOB-SNPs, we used a fluorescence navigation endoscopy system, FIONavi4K, which has been used in surgery. After intraperitoneal administration of FA-IR780&PFOB-SNPs at a dosage of 10 mg/kg, the mice bearing SKOV3 subcutaneous tumours underwent surgery at 72 h, and the operation areas were exposed to the FIONavi4K system. Real-time images were recorded during surgery. IR780-loaded folate-targeted ordinary nanoparticles (fluorescence always on and without PLGA-PEOz) were used as the control group as above. As shown in Figure 6A, both the FA-IR780&PFOB-SNPs and control groups showed enhanced fluorescence signals in tumours, but the background fluorescence signal in the control group was higher than that in the FA-IR780&PFOB-SNPs group. Quantitative analysis of the TBRs showed that the TBR of FA-IR780&PFOB-SNPs was 3.05 ± 0.15 , which was significantly higher than that of the control group (2.24 ± 0.15) (Figure 6B). H&E staining further confirmed that the fluorescent tissues were cancerous tissues (Figure 6C). These results confirmed the intraoperative imaging feasibility of FA-IR780&PFOB-SNPs, which had higher TBRs compared to the ordinary nanoparticles (fluorescence always on).

Because of the characteristics of peritoneal implantation metastases, many metastases with different sizes (from submillimetre to large scales) could form in abdominal organs, including the peritoneum, intestines and liver, in patients

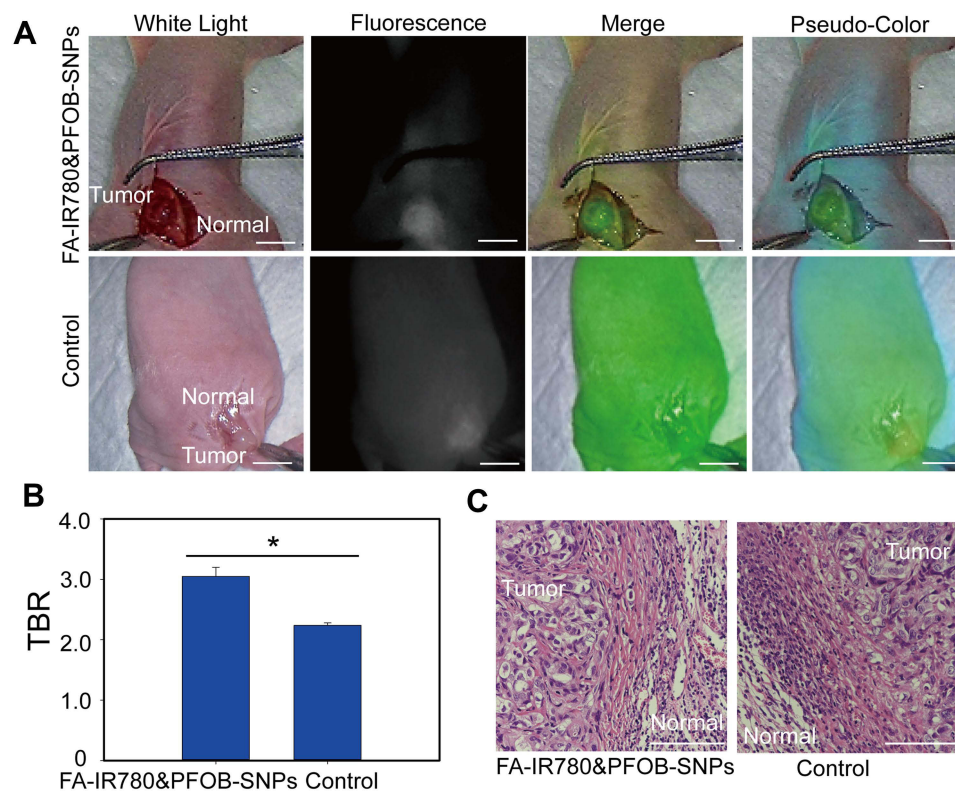


Figure 6 Intraoperative navigation of SKOV3 subcutaneous tumours by FA-IR780&PFOB-SNPs in vivo. **(A)** Intraoperative real-time monitoring with a fluorescence navigation endoscopy system (FIONavi4K) at 72 h after the intraperitoneal administration of FA-IR780&PFOB-SNPs and control. The bars represent 1 cm. **(B)** The mean fluorescence signal intensities in tumours and surrounding normal tissues (TBR) of the FA-IR780&PFOB-SNPs group and control group. (* $P < 0.05$). **(C)** H&E staining observed in the fluorescence images of tumours and normal tissue cross-sections. The bar represents 50 μ m. Values are expressed as the mean \pm SD, $n = 3$ per group.

with ovarian cancer. Unfortunately, due to the absence of symptoms and lack of screening, peritoneal implantation metastasis often occurs in over 75% of patients with newly diagnosed ovarian cancer. For ovarian cancer patients, finding metastatic lesions, clearly delineating tumour boundaries, and performing complete resection are key to a favourable prognosis. Therefore, we established ovarian intraperitoneal xenograft tumour models to explore the capability of FA-IR780&PFOB-SNPs to display intraperitoneal metastatic tumours during surgery with a fluorescence navigation endoscopy system (FIONavi4K). After intraperitoneal administration of FA-IR780&PFOB-SNPs at a dosage of 10 mg/kg, the mice bearing SKOV3 intraperitoneal xenograft tumours underwent surgery at 72 h, and the operation areas were exposed to the FIONavi4K. Real-time images were recorded during surgery. IR780-loaded folate-targeted ordinary nanoparticles (fluorescence always on and without PLGA-PEOz) were used as the control group as above. As shown in Figure 7A, tumours with maximum diameters of approximately 2 cm could be observed in the surgical areas via the white light mode, but the boundaries between the tumours and surrounding normal tissues were not clear. However, the tumour boundaries could clearly be delineated when using the fluorescence mode since the fluorescence signals in the tumour areas were much stronger than those in the surrounding normal tissues. In the control group, although the tumour regions

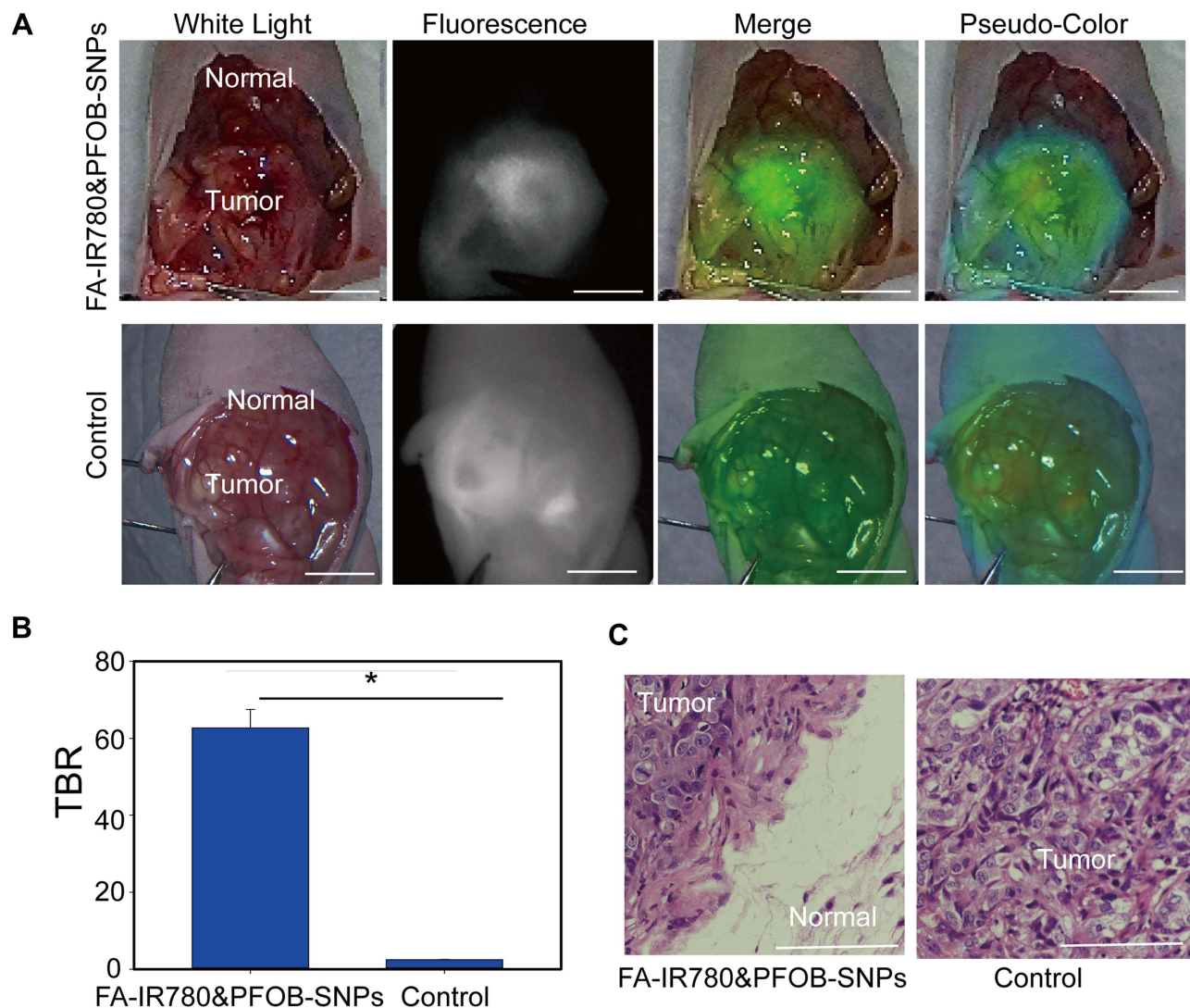


Figure 7 Intraoperative navigation for SKOV3 abdominal metastases by FA-IR780&PFOB-SNPs in vivo. **(A)** Intraoperative real-time monitoring with FIONavi4K at 72 h after the intraperitoneal administration of FA-IR780&PFOB-SNPs and control. The bars represent 1 cm. **(B)** The mean fluorescence signal intensities in tumours and surrounding normal tissues (TBR) of the FA-IR780&PFOB-SNPs group and control group. (* $P < 0.05$). **(C)** H&E staining results as shown in the fluorescence images of the cross-sections of tumours and normal tissue. The bar represents 50 μ m. Values are expressed as the mean \pm SD, $n = 3$ per group.

displayed stronger fluorescence signals than the normal tissues, the boundaries were not clear due to the considerable fluorescence signals from the surrounding normal tissues. Quantitative analysis of the TBRs showed that the TBR of the FA-IR780&PFOB-SNPs group was 62.71 ± 4.84 , which was much higher than that of the control group (2.45 ± 0.07) (Figure 7B). The tumours were resected through fluorescence image-guided H&E staining. H&E staining further confirmed that the fluorescent tissues were cancerous tissues (Figure 7C). Notably, the boundaries between tumours and normal tissues could also be observed under the microscope in the FA-IR780&PFOB-SNPs group. These results confirmed that FA-IR780/PFOB-SNP-mediated intraoperative near-infrared fluorescence imaging could accurately delineate tumour boundaries and guide the complete resection of peritoneal implantation metastases. Moreover, the TBRs in ovarian intraperitoneal xenograft tumour models were much higher than those in ovarian subcutaneous xenograft tumour models (62.71 ± 4.84 vs 3.05 ± 0.15), which suggested that FA-IR780&PFOB-SNPs may be more suitable for intraperitoneal tumours (especially ovarian cancer). We suspected that the nanoparticle stayed in the abdominal cavity for a long time through intraperitoneal injection, actively targeted to the tumour through IR780 and folic acid, disassembled at the tumor site, released IR780, and the tumours were displayed by fluorescence. Meanwhile, the accumulation of FA-IR780&PFOB-SNPs in normal tissues was less and the fluorescence was quenched, which greatly improved the TBR.

For ovarian cancer patients, the removal of micrometastatic lesions during surgery is another key factor to establish a favourable prognosis.²⁷ In traditional laparotomy, the search for tumours often relies on the surgeon's experience, touch and vision, and these subjective judgements and sensory limitations often result in residual microlesions.⁴ Moreover, laparoscopic surgery and robotic surgery are increasingly widely used in the field of gynaecology. Compared with traditional laparotomy, laparoscopic surgery and robotic surgery have the advantages of less trauma, multiangle intuitive vision, quicker postoperative recovery and shorter hospital stays.²⁸ However, in laparoscopic surgery and robotic surgery, surgeons cannot detect tumours by touch. Therefore, it is necessary to improve the prognosis for ovarian cancer patients by intuitively displaying small tumour lesions and by performing satisfactory R0 resections through tumour-targeting fluorescent probes. In our study, we found that in mouse ovarian intraperitoneal xenograft tumour models, metastases with maximum diameters less than 2 mm could be detected by FA-IR780&PFOB-SNPs mediated near infrared fluorescence imaging, as shown in Figure 8A. The intensities of the NIR fluorescence signals were also quantitatively analysed by ImageJ software. The average fluorescence intensity of tumour tissues was 91.17 ± 1.79 and that of the surrounding normal tissues was 12.72 ± 3.63 .

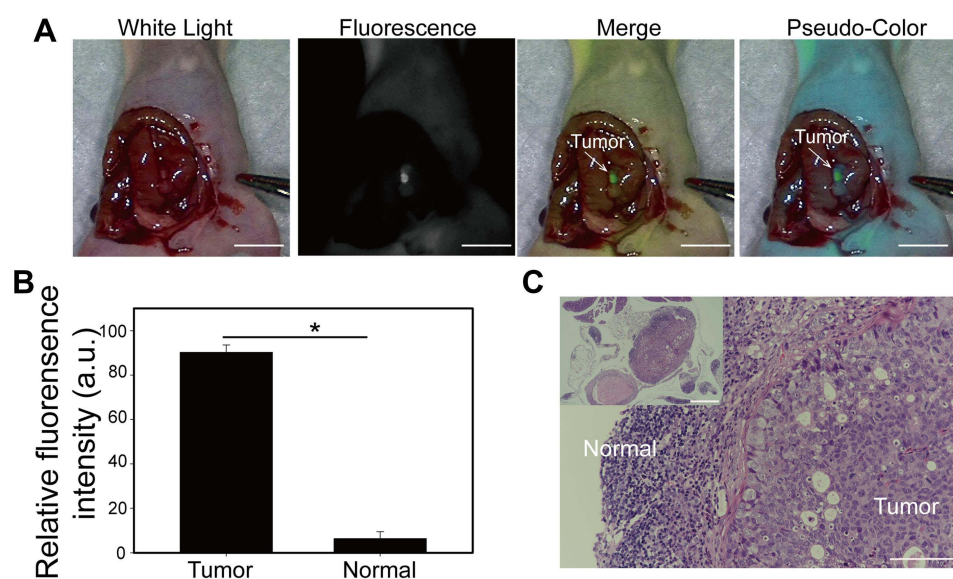


Figure 8 Intraoperative navigation of SKOV3 micrometastases by FA-IR780&PFOB-SNPs in vivo. (A) Intraoperative real-time monitoring by FIONavi4K at 72 h after intraperitoneal administration of FA-IR780&PFOB-SNPs. The bars represent 1 cm. (B) The mean fluorescence intensities of the tumours and adjacent normal tissues in Panel A (* $P < 0.05$). (C) H&E staining of fluorescence images of cross-sections of tumours and normal tissues. The bars represent 50 μ m. Values are expressed as the mean \pm SD, $n = 3$ per group.

The ratio of the average fluorescence intensity of tumour tissue to that of the surrounding normal tissue (TBR) was approximately 7.62 ± 2.07 , which indicated that the fluorescence signal intensities in tumour tissue were much higher than those in the surrounding normal tissue (Figure 8B). Through the guidance of intraoperative real-time near infrared fluorescence images by FIONavi4K, the microlesions were removed for further pathological analysis. As shown in Figure 8C, as observed under the microscope, the actual maximum diameter of the micrometastatic lesions was less than $250 \mu\text{m}$, and these were surrounded by normal tissues. Our study found that the FA-IR780&PFOB-SNPs mediated NIR fluorescence navigation system can clearly display micron-level metastases, and the intraoperative borders of tumour lesions are larger than the actual tumour lesions, which is very important for intraoperative tumour resection to achieve R0.²⁷

Conclusion

On the basis of previous studies, we successfully optimized IR780-loaded folate-targeted nanoparticles by using the pH response nano framework (FA- PEG-PLGA-PEOz) and by adjusting the dosage of IR780 (FA-IR780&PFOB-SNPs), which improved the NIR fluorescence ability for displaying ovarian tumours. FA-IR780&PFOB-SNPs have been demonstrated to disintegrate and the NIR fluorescence turn on in acidic tumour microenvironments while integrating and the NIR fluorescence turn off in neutral normal tissue due to the aggregate fluorescence self-quenching effect of IR780 and the pH response. When comparing the NIR fluorescence imaging effect of nanoparticles in peritoneal metastatic tumour models and subcutaneous xenograft tumour models, we found that FA-IR780&PFOB-SNPs are more suitable for ovarian cancer, whose main metastatic method is peritoneal implantation. The TBR was 62.71 ± 4.84 in peritoneal metastatic tumour models, which was much higher than that in subcutaneous xenograft tumour models (3.05 ± 0.15). Even for microscale peritoneal metastatic lesions, the TBRs could exceed 5.0 (7.62 ± 2.07). This is very important for ovarian cancer patients because it could be intraoperative specific to reveal occult micrometastases, enable precise navigational tumour resection, and result in improved prognoses.¹⁶

Acknowledgments

This work was financially supported by the China Postdoctoral Science Foundation (Grant No. 2019M663281) and Basic and Applied Basic Research Fund of Guangdong Province (Grant No. 2020A151511091).

Disclosure

The authors report no conflicts of interest in this work.

References

1. Siegel RL, Miller KD, Fuchs HE, et al. Cancer statistics, 2021. *CA-A Cancer J Clin*. 2021;71(1):7–33. doi:10.3322/caac.21654
2. Lheureux S, Braunstein M, Oza AM. Epithelial ovarian cancer: evolution of management in the era of precision medicine. *CA Cancer J Clin*. 2019;69(4):280–304. doi:10.3322/caac.21559
3. Du Bois A, Reuss A, Pujade-Lauraine E, et al. Role of surgical outcome as prognostic factor in advanced epithelial ovarian cancer: a combined exploratory analysis of 3 prospectively randomized Phase 3 multicenter trials: by the Arbeitsgemeinschaft Gynaekologische Onkologie Studiengruppe Ovarialkarzinom (AGO-OVAR) and the Groupe d'Investigateurs Nationaux Pour les Etudes des Cancers de l'Ovaire (GINECO). *Cancer*. 2009;115(6):1234–1244. doi:10.1002/cncr.24149
4. Hacker NF, Rao A. Surgery for advanced epithelial ovarian cancer. *Best Pract Res Clin Obstet Gynaecol*. 2017;41:71–87. doi:10.1016/j.bpobgyn.2016.10.007
5. Lakhman Y, Akin O, Sohn MJ, et al. Early postoperative CT as a prognostic biomarker in patients with advanced ovarian, tubal, and primary peritoneal cancer deemed optimally debulked at primary cytoreductive surgery. *AJR Am J Roentgenol*. 2012;198(6):1453–1459. doi:10.2214/AJR.11.7257
6. Low PS, Singhal S, Srinivasarao M. Fluorescence-guided surgery of cancer: applications, tools and perspectives. *Curr Opin Chem Biol*. 2018;45:64–72. doi:10.1016/j.cbpa.2018.03.002
7. Abu-Rustum NR, Angioli R, Bailey AE, et al. IGCS Intraoperative Technology Taskforce. Update on near infrared imaging technology: beyond white light and the naked eye, indocyanine green and near infrared technology in the treatment of gynecologic cancers. *Int J Gynecol Cancer*. 2020;30(5):670–683. doi:10.1136/ijgc-2019-001127
8. Van Manen L, Handgraaf HJM, Diana M, et al. A practical guide for the use of indocyanine green and methylene blue in fluorescence-guided abdominal surgery. *J Surg Oncol*. 2018;118(2):283–300. doi:10.1002/jso.25105
9. Veys I, Pop FC, Vankerckhove S, et al. ICG-fluorescence imaging for detection of peritoneal metastases and residual tumoral scars in locally advanced ovarian cancer: a pilot study. *J Surg Oncol*. 2018;117(2):228–235. doi:10.1002/jso.24807
10. Vankayala R, Bahena E, Guerrero Y, et al. Virus-mimicking nanoparticles for targeted near infrared fluorescence imaging of intraperitoneal ovarian tumors in mice. *Ann Biomed Eng*. 2021;49(2):548–559. doi:10.1007/s10439-020-02589-8

11. Burns JM, Shafer E, Vankayala R, et al. Near infrared fluorescence imaging of intraperitoneal ovarian tumors in mice using erythrocyte-derived optical nanoparticles and spatially-modulated illumination. *Cancers*. 2021;13(11):2544. doi:10.3390/cancers13112544
12. Ravoori MK, Singh S, Bhavane R, et al. Multimodal magnetic resonance and near-infrared-fluorescent imaging of intraperitoneal ovarian cancer using a dual-mode-dual-gadolinium liposomal contrast agent. *Sci Rep*. 2016;6:38991. doi:10.1038/srep38991
13. Guerrero Y, Singh SP, Mai T, et al. Optical characteristics and tumor imaging capabilities of near infrared dyes in free and nano-encapsulated formulations comprised of viral capsids. *ACS Appl Mater Interfaces*. 2017;9(23):19601–19611. doi:10.1021/acsami.7b03373
14. Hoogstins CE, Tummers QR, Gaarenstroom KN, et al. A novel tumor-specific agent for intraoperative near-infrared fluorescence imaging: a translational study in healthy volunteers and patients with ovarian cancer. *Clin Cancer Res*. 2016;22(12):2929–2938. doi:10.1158/1078-0432.CCR-15-2640
15. Randall LM, Wenham RM, Low PS, et al. A Phase II, multicenter, open-label trial of OTL38 injection for the intraoperative imaging of folate receptor-alpha positive ovarian cancer. *Gynecol Oncol*. 2019;155(1):63–68. doi:10.1016/j.ygyno.2019.07.010
16. Mangeolle T, Yakavets I, Marchal S, et al. Fluorescent nanoparticles for the guided surgery of ovarian peritoneal carcinomatosis. *Nanomaterials*. 2018;8(8):572. doi:10.3390/nano8080572
17. Scaranti M, Cojocaru E, Banerjee S, et al. Exploiting the folate receptor α in oncology. *Nat Rev Clin Oncol*. 2020;17(6):349–359. doi:10.1038/s41571-020-0339-5
18. Song J, Zhang N, Zhang L, et al. IR780-loaded folate-targeted nanoparticles for near-infrared fluorescence image-guided surgery and photothermal therapy in ovarian cancer. *Int J Nanomedicine*. 2019;14:2757–2772. doi:10.2147/IJN.S203108
19. Li X, Schumann C, Albarqi HA, et al. A tumor-activatable theranostic nanomedicine platform for NIR fluorescence-guided surgery and combinatorial phototherapy. *Theranostics*. 2018;8(3):767–784. doi:10.7150/thno.21209
20. Hernot S, Van Manen L, Debie P, et al. Latest developments in molecular tracers for fluorescence image-guided cancer surgery. *Lancet Oncol*. 2019;20(7):e354–e67. doi:10.1016/S1470-2045(19)30317-1
21. Wang D, Zhou Y, Li X, et al. Mechanisms of pH-sensitivity and cellular internalization of PEOz-b-PLA micelles with varied hydrophilic/hydrophobic ratios and intracellular trafficking routes and fate of the copolymer. *ACS Appl Mater Interfaces*. 2017;9(8):6916–6930. doi:10.1021/acsami.6b16376
22. Danhier F, Ansorena E, Silva JM, et al. PLGA-based nanoparticles: an overview of biomedical applications. *J Control Release*. 2012;161(2):505–522. doi:10.1016/j.jconrel.2012.01.043
23. Song J, Zhang L, Yi H, et al. NIR-responsive nanoplatform for pre/intraoperative image-guided carcinoma surgery and photothermal ablation of residual tumor tissue. *Nanomedicine*. 2019;20:102020. doi:10.1016/j.nano.2019.102020
24. Colby AH, Berry SM, Moran AM, et al. Highly specific and sensitive fluorescent nanoprobe for image-guided resection of sub-millimeter peritoneal tumors. *ACS nano*. 2017;11(2):1466–1477. doi:10.1021/acsnano.6b06777
25. Wang Y, Liu T, Zhang E, et al. Preferential accumulation of the near infrared heptamethine dye IR-780 in the mitochondria of drug-resistant lung cancer cells. *Biomaterials*. 2014;35(13):4116–4124. doi:10.1016/j.biomaterials.2014.01.061
26. Zhang L, Yi H, Song J, et al. Mitochondria-targeted and ultrasound-activated nanodroplets for enhanced deep-penetration sonodynamic cancer therapy. *ACS Appl Mater Interfaces*. 2019;11(9):9355–9366. doi:10.1021/acsami.8b21968
27. Kurmit KC, Fleming GF, Lengyel E. Updates and new options in advanced epithelial ovarian cancer treatment. *Obstet Gynecol*. 2021;137(1):108–121. doi:10.1097/AOG.0000000000004173
28. Muaddi H, Hafid ME, Choi WJ, et al. Clinical outcomes of robotic surgery compared to conventional surgical approaches (laparoscopic or open): a systematic overview of reviews. *Annals Surg*. 2021;273(3):467–473.